Physics-Informed Operator Learning for Real-Time Battery State Estimation and Health Monitoring

Alexander Gabriel Harej[1], Marco Giglio[2], Francesco Cadini[3]

[1,2,3] *Politecnico di Milano, Dipartimento di Meccanica, Via La Masa, 1, Milano, 20156, MI, Italy*
alexandergabriel.harej@polimi.it
francesco.cadini@polimi.it
marco.giglio@polimi.it

ABSTRACT

The increasing demand for reliable and safe lithium-ion (Li-ion) battery packs in the automotive sector has intensified the need for advanced diagnostics and prognostics capabilities within next-generation Battery Management Systems (BMSs). A key BMS function is the estimation of the battery State of Charge (SOC) and State of Health (SOH), typically achieved through Kalman-based observers that require an explicit state-space representation of the cell. Equivalent Circuit Models (ECMs), while computationally efficient, are fundamentally empirical constructs that offer limited physical insight and poor generalization outside their identification range. Electrochemical Models (EMs), by contrast, capture the underlying reaction kinetics, mass transport, and diffusion processes governing cell behavior, enabling higher fidelity across a broader range of operating conditions at the cost of computational complexity that has, so far, precluded their real-time deployment within BMS observers. This work addresses this barrier by relying on a physics-informed surrogate of the Single Particle Model (SPM), based on a Multiple-Input Operator Network (MIONet) that directly encodes the SPM governing equations into a compact, real-time-executable state-space representation. The resulting EM-based observer is embedded within an Unscented Kalman Filter (UKF) for the joint estimation of SOC and SOH, where SOH is represented by the Loss of Lithium Inventory (LLI, in moles) augmented to the SPM concentration state. The framework is validated on a high-fidelity Doyle-Fuller-Newman (DFN) plant including electrochemically resolved Solid Electrolyte Interphase (SEI) growth, lithium plating, and loss of active material, simulated in PyBaMM. Six case studies covering Constant Current-Constant Voltage (CC-CV) charges followed by CC and Dynamic Stress Test (DST) discharges at $10°C$, $25°C$, and $40°C$ are considered, in which the cell is cycled to its end-of-life (EOL, 80% of initial capacity). Quantitative comparisons against an ECM-based observer with an identical joint-UKF structure show that the EM-based observer consistently delivers lower SOC and SOH Root Mean Square Error (RMSE) and substantially better-calibrated confidence intervals (measured via the Coverage Width-based Criterion, CWC). The largest advantage is observed under highly dynamic load profiles, establishing the proposed approach as a viable pathway toward high-fidelity, real-time diagnosis in next-generation BMSs.

1. INTRODUCTION

In recent years, electric vehicles (EVs) have experienced rapid growth driven by environmental, economic, and technological factors (Alanazi, 2023). Li-ion batteries are one of the most expensive and safety-critical components of an EV. This makes it essential to use them efficiently and to extend their lifespan by mitigating degradation and avoiding hazards such as thermal runaway. These objectives can only be met by an advanced Battery Management System (BMS) (Hu, Xu, Lin, & Pecht, 2020), whose core function is the continuous, real-time monitoring of the internal state of each cell.

Two states are of particular importance: the State of Charge (SOC), which describes the amount of usable charge currently stored in the cell, and the State of Health (SOH), which quantifies the cell's degradation with respect to its beginning-of-life condition. Neither can be measured directly with on-board sensors, and both must therefore be inferred from terminal voltage, load current, and surface temperature. Crucially, SOC and SOH are not independent quantities. The SOC is conventionally defined as the ratio between the residual charge and the actual (aged) capacity of the cell; consequently, any error or drift in the capacity estimate translates one-to-one into a bias in the SOC. Conversely, most online SOH update rules rely on a consistent reconstruction of the charge throughput between two well-defined SOC anchors, so that an inaccurate SOC estimate directly degrades the SOH update. The two states can thus be seen as mutually reinforc-

ing: an accurate SOC estimate is a prerequisite for tracking SOH, while an up-to-date SOH is needed for an accurate, unbiased SOC. A consistent and stable monitoring scheme therefore requires a co-estimation framework in which SOC and SOH are recursively refined together within a single observer.

State and health estimation techniques can be broadly classified into three families (Hu et al., 2020): ad-hoc laboratory tests, purely data-driven methods, and model-based estimators. The first family relies on dedicated characterization tests that provide highly accurate references but require specialized hardware and long offline interruptions, making them unsuitable for online deployment (Nuroldayeva, Serik, Adair, Uzakbaiuly, & Bakenov, 2023). The second family employs neural networks to map measurable signals directly to the target SOC or SOH (Zhang et al., 2018). Such black-box estimators are computationally cheap once trained, but they require very large datasets and tend to extrapolate poorly outside their training distribution. The third family, on which the present work focuses, is composed of model-based estimators in which a mathematical model of the cell is embedded into a closed-loop observer (typically a Kalman filter) (Hu et al., 2020).

State-of-the-art industrial BMSs largely rely on phenomenological Equivalent Circuit Models (ECMs) (Krewer et al., 2018), in which the cell dynamics are reproduced by empirical Resistance-Capacitance (RC) networks. ECMs are computationally inexpensive, but their parameters do not have a direct physical meaning, require extensive offline characterization, and tend to lose accuracy under highly dynamic transients (Chaturvedi, Klein, Christensen, Ahmed, & Kojic, 2010). Most importantly, they do not provide any direct access to localized electrochemical phenomena, which forces manufacturers to adopt conservative, oversized designs. The research trend is therefore shifting toward physics-based Electrochemical Models (EMs), and in particular toward the Doyle-Fuller-Newman (DFN) framework (Doyle, Fuller, & Newman, 1993), which describes the lithium concentration and potential in the solid and liquid phases via a system of Partial Differential Equations (PDEs). Solving the DFN online is prohibitive for current BMS hardware, and Model Order Reduction (MOR) techniques are commonly applied. The most popular MOR variant is the Single Particle Model (SPM) (Marquis, Sulzer, Timms, Please, & Chapman, 2019), which is typically discretized by Finite Difference, Finite Volume, or spectral approximations. Even in their most streamlined forms, however, these techniques still introduce a non-negligible computational overhead.

A promising alternative is offered by the recent intersection of scientific computing and deep learning. Operator-learning architectures such as the Multiple-Input Operator Network (MIONet) (Jin, Meng, & Lu, 2022) can learn the solution operator of a PDE directly from physics, without recourse to numerical solvers. When trained in a physics-informed setting via Physics-Informed Neural Networks (PINNs), these networks evaluate the future state of the system in a single forward pass, which is ideally suited for real-time embedded deployment. In previous work (Brancato, Harej, Giglio, & Cadini, 2026), we developed and validated a physics-informed MIONet surrogate of the SPM and embedded it into a UKF for SOC estimation, demonstrating its accuracy and computational efficiency against ECM-based observers under a variety of load profiles, temperatures, and chemistries.

The present work extends the MIONet-SPM framework to the joint estimation of SOC and SOH. We demonstrate that a physics-informed surrogate coupled with a joint Kalman filter can simultaneously track fast-scale concentration dynamics and slow-scale capacity fade, bypassing the need for empirical degradation models. Performance is directly benchmarked against a State-of-the-Art (SOA) ECM. The main contributions are:

- A **Joint UKF Formulation** that co-estimates the electrodes' spatial lithium concentrations (dictating SOC) and the LLI (dictating SOH) within a single augmented state vector.
- An **Implicit SOH Update Mechanism** that tracks capacity fade without complex empirical aging submodels. Instead, the UKF dynamically corrects the LLI state driven entirely by the terminal voltage residual, exploiting the electrochemical model's natural sensitivity to lithium loss.
- A **Comprehensive Validation and Benchmark** against a high-fidelity DFN plant simulating realistic aging (SEI growth, lithium plating, and loss of active material). The framework is evaluated over full-lifecycle case studies (constant and DST profiles at $10°C$, $25°C$, and $40°C$) and benchmarked against an SOA ECM to prove its superior accuracy and robustness.

The remainder of the paper is organized as follows. Section 2 recalls the SPM formulation, summarizes the MIONet surrogate, and presents the proposed joint UKF. Section 3 describes the DFN plant, the ECM baseline, and the validation protocol. Section 4 discusses the results of the six case studies. Section 5 closes the paper and outlines future research directions.

2. METHODOLOGY

2.1. Electrochemical Model

A Li-ion cell consists of a negative electrode (anode), a porous separator, and a positive electrode (cathode), all sandwiched between two current collectors. Active material particles within each electrode store lithium, while the liquid electrolyte facilitates ion transport during charging and discharging. During discharge, a lithium atom intercalated within the anode oxidizes, releasing an electron to the negative current collector. This electron travels through an external circuit to

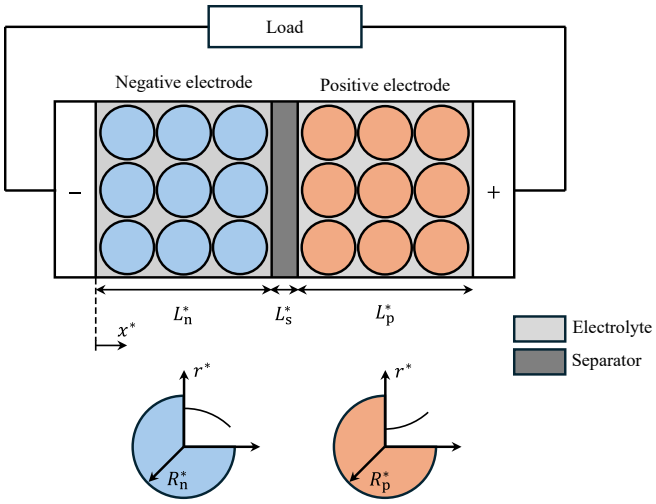

Figure 1. Schematic representation of the DFN model domains, reduced to the representative spherical particles in the SPM.

power a load, while the newly formed lithium ion (Li^+) migrates internally through the electrolyte toward the cathode, where it recombines with the electron and intercalates into the positive active material. The relative amount of lithium currently stored within the electrode particles determines the instantaneous SOC. Conversely, the total amount of cyclable lithium available in the entire system determines the SOH.

To model these coupled dynamics, the SPM reduces the macroscopic complexity of the cell by treating the negative and positive electrodes as individual, representative spherical particles of radii R_n and R_p (Fig. 1). A fundamental assumption of the SPM is that the transport of lithium ions in the liquid electrolyte is infinitely fast, allowing electrolyte concentration gradients and associated potential drops to be neglected. Consequently, the primary dynamic bottleneck of the system is the solid-phase diffusion within the active material. The transport of lithium inside these solid particles is governed by Fick's second law in spherical coordinates, which in its non-dimensional form reads, for each electrode $\mathrm{k} \in \{\mathrm{n}, \mathrm{p}\}$:

$$\mathcal{C}_\mathrm{k} \frac{\partial c_{\mathrm{s,k}}}{\partial t} = \frac{1}{r_\mathrm{k}^2} \frac{\partial}{\partial r_\mathrm{k}} \left(r_\mathrm{k}^2 \frac{\partial c_{\mathrm{s,k}}}{\partial r_\mathrm{k}} \right) \tag{1}$$

where $c_{\mathrm{s,k}}(r,t)$ is the solid concentration normalized by the maximum theoretical concentration $c_{\mathrm{s,k,max}}$, $r_\mathrm{k} \in [0,1]$ is the normalized radial coordinate, and $\mathcal{C}_\mathrm{k}$ is a non-dimensional time constant depending on the solid diffusion coefficient $D_{\mathrm{s,k}}$. Spherical symmetry at the center of the particle and the intercalation flux at the surface, driven by the applied current $I(t)$, define the boundary conditions:

$$\left. \frac{\partial c_{\mathrm{s,k}}}{\partial r_\mathrm{k}} \right|_{r_\mathrm{k}=0} = 0 \tag{2}$$

$$-\frac{a_\mathrm{k}\gamma_\mathrm{k}}{\mathcal{C}_\mathrm{k}} \left. \frac{\partial c_{\mathrm{s,k}}}{\partial r_\mathrm{k}} \right|_{r_\mathrm{k}=1} = \pm \frac{I(t)}{L_\mathrm{k}} \tag{3}$$

where a_k is the volumetric interfacial area per unit volume, γ_k is the stoichiometric normalization factor, and L_k is the electrode thickness.

The terminal voltage $V(t)$ is then computed algebraically from the surface concentrations through the Open-Circuit Voltages (OCV), U_p and U_n, and the reaction overpotentials η_p and η_n:

$$V(t) = U_\mathrm{p}\big(c_{\mathrm{s,p}}|_{r_\mathrm{p}=1}\big) - U_\mathrm{n}(c_{\mathrm{s,n}}|_{r_\mathrm{n}=1}) - \eta_\mathrm{p} - \eta_\mathrm{n} \tag{4}$$

Assuming symmetric charge-transfer coefficients, the Butler-Volmer equation can be analytically inverted to express each overpotential as:

$$\eta_\mathrm{k} = \frac{2RT}{F} \sinh^{-1}\left(\frac{I(t)}{2a_\mathrm{k}L_\mathrm{k}j_{0,\mathrm{k}}(c_{\mathrm{s,k}}|_{r=1})} \right) \tag{5}$$

In the context of the SPM, the applied macroscopic load current $I(t)$ acts as the known deterministic input, the spatially distributed lithium concentrations within the spherical electrode particles represent the internal hidden states, and the terminal voltage $V(t)$ serves as the measurable output signal. Therefore, given an arbitrary current profile, the SPM analytically computes the corresponding terminal voltage of the Li-ion battery cell.

2.2. Physics-Informed MIONet Surrogate

The MIONet surrogate of the SPM used as the state-transition function of the EM-based observer has been introduced and characterized in detail in (Brancato et al., 2026); we summarize here only the elements that are strictly necessary for the joint-filter formulation. The network learns the discrete-time solution operator mapping a current spatial concentration profile and the applied current onto the concentration profile at the next time step:

$$\hat{c}_{\mathrm{s,k}}(\,\cdot\,, t_{n+1}) = \mathcal{G}_{\boldsymbol{\theta}}(c_{\mathrm{s,k}}(\,\cdot\,, t_n),\, I(t_n))\,, \tag{6}$$

The MIONet architecture consists of two branch networks, encoding the spatial concentration profile and the scalar applied current, and a trunk network encoding the spatio-temporal coordinates (r,t) at which the future state is evaluated (Fig. 2). The continuous prediction is reconstructed as:

$$\hat{c}_{\mathrm{s,k}}(r,t) = \sum_{j=1}^{p} \left[b_{1,j}(c_{\mathrm{s,k}}) \cdot b_{2,j}(I) \right] \cdot t_j(r,t) \tag{7}$$

The MIONet is trained without any labeled data: a physics-

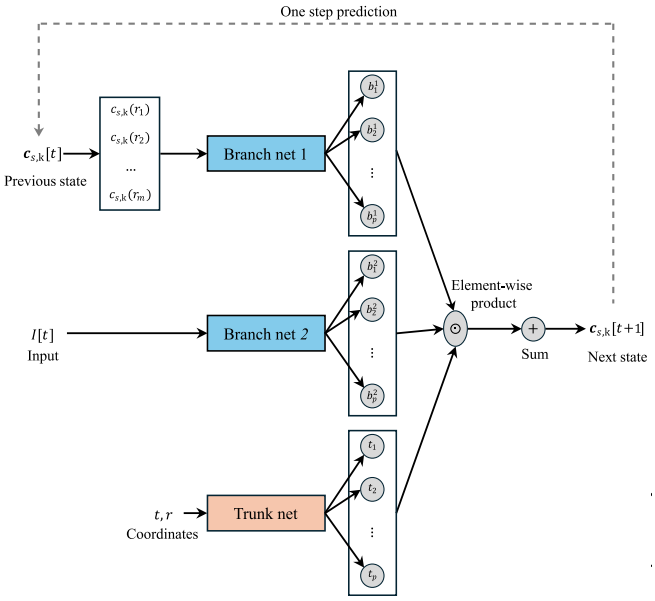

Figure 2. MIONet architecture used as state-transition function: two branch networks encode the spatial concentration profile and the applied current, while a trunk network encodes the spatio-temporal query coordinates. The output is the predicted concentration profile at the next time step.

informed loss is built from the residuals of Eqs. (1)-(3) together with the initial condition:

$$L = \lambda_{\text{PDE}} L_{\text{PDE}} + \lambda_{\text{BC}} L_{\text{BC}} + \lambda_{\text{IC}} L_{\text{IC}}, \tag{8}$$

and the training inputs (initial concentration profiles and current sequences) are sampled from Gaussian Random Fields (GRFs) and Gaussian distributions to span a representative portion of the operating envelope. Optimization is performed with a combined Adam/L-BFGS strategy. We refer the reader to (Brancato et al., 2026) for the complete training procedure and convergence analysis.

2.3. Joint UKF for SOC and SOH Co-Estimation

The proposed estimator is a single UKF (Wan & Van Der Merwe, 2000) acting on an augmented state vector that combines the fast electrochemical dynamics of the SPM and the slow dynamics of the cell capacity fade. To embed the SPM into the observer, its state-space representation is formulated using the trained MIONet. The two concentrations of Li-ions in the electrodes serve as the primary system states. Discretized along the radial coordinate into vectors $\mathbf{c}_{s,\text{p}}$ and $\mathbf{c}_{s,\text{n}}$, the state transition at time step $t+1$ depends on the concentrations and the load current density I at the previous time step t:

$$\mathbf{c}_s[t+1] = \begin{pmatrix} \mathbf{c}_{s,\text{p}}[t+1] \\ \mathbf{c}_{s,\text{n}}[t+1] \end{pmatrix} = \begin{pmatrix} f_{\text{p}}\left(\mathbf{c}_{s,\text{p}}[t], I[t], \Delta t\right) \\ f_{\text{n}}\left(\mathbf{c}_{s,\text{n}}[t], I[t], \Delta t\right) \end{pmatrix} \tag{9}$$

$$V[t+1] = h\left(\mathbf{c}_s[t], I[t]\right) \tag{10}$$

where f_{p} and f_{n} are the two non-linear state transition functions surrogated by the MIONets, and h is the analytical SPM terminal voltage measurement function (4).

2.3.1. Augmented State Vector

To achieve joint estimation of both SOC and SOH, the fast block of the state vector is augmented with a slow-scale parameter: the LLI, Δn_{Li}, expressed in moles. The full augmented state vector reads:

$$\mathbf{x}_k^{\text{EM}} = \begin{bmatrix} \mathbf{c}_{s,\text{p}} \\ \mathbf{c}_{s,\text{n}} \\ \Delta n_{\text{Li}} \end{bmatrix}_k \tag{11}$$

The LLI evolves as a slow random walk between consecutive samples:

$$\Delta n_{\text{Li},k+1} = \Delta n_{\text{Li},k} + w_{\text{LLI},k} \tag{12}$$

where $w_{\text{LLI},k}$ is a zero-mean Gaussian process noise. The variance of this noise is set several orders of magnitude smaller than the process noise on the concentration block, enforcing the physical reality that LLI is quasi-constant on the fast time scale of a single discharge cycle. The augmented state vector transition function is therefore:

$$\mathbf{c}_s[t+1] = \begin{pmatrix} \mathbf{c}_{s,\text{p}}[t+1] \\ \mathbf{c}_{s,\text{n}}[t+1] \end{pmatrix} = \begin{pmatrix} f_{\text{p}}\left(\mathbf{c}_{s,\text{p}}[t], I[t], \Delta t\right) \\ f_{\text{n}}\left(\mathbf{c}_{s,\text{n}}[t], I[t], \Delta t\right) \end{pmatrix} \tag{13}$$

$$\Delta n_{\text{Li}}[t+1] = \Delta n_{\text{Li}}[t] + w_{\text{LLI}} \tag{14}$$

Once the LLI is estimated, the SOH is directly extracted as an algebraic function of the remaining cyclable lithium:

$$\text{SOH}_k = 1 - \frac{\Delta n_{\text{Li},k} \cdot F}{Q_{\text{nom}}} \tag{15}$$

where F is the Faraday constant and Q_{nom} is the nominal capacity at the beginning of life.

A critical challenge in joint estimation is ensuring that the estimated LLI remains physically consistent with the estimated concentration profiles. To enforce this, we implement a specific algorithmic constraint within the UKF utilizing the Unscented Transform (UT). In addition to the terminal voltage V_k, the UKF utilizes a second, virtual measurement: the total initial amount of cyclable lithium at the beginning of life, $n_{\text{Li},0}$.

At any given instant, the total cyclable lithium must be strictly partitioned and conserved between three pools:

$$n_{\text{Li},0} = n_{\text{Li,a}}(t) + n_{\text{Li,c}}(t) + \Delta n_{\text{Li}}(t) \tag{16}$$

where $n_{\text{Li,a}}$ and $n_{\text{Li,c}}$ are the moles of lithium inside the active material of the anode and cathode, respectively. These values are computed dynamically by the UKF by integrating the estimated spatial concentration profiles ($\mathbf{c}_{s,\text{n}}$ and $\mathbf{c}_{s,\text{p}}$) over their respective particle volumes.

By treating $n_{\text{Li},0}$ as a fixed, known measurement within the

UKF's measurement update step, the filter is mathematically forced to balance the state vector. A voltage residual that the filter cannot accommodate by adjusting the concentration gradients alone is subsequently absorbed by a reallocation of lithium between the active pools and the SEI, directly updating Δn_{Li}.

2.3.2. Online Parameter Updating and SOC Computation

One of the most significant advantages of utilizing a physics-based EM over a traditional ECM is the ability to directly update internal physical parameters as the battery ages. As lithium is permanently lost to the SEI layer, the physical boundary limits of the electrodes, specifically, the maximum and minimum stoichiometries ($c_{s,\mathrm{k}}|_{\mathrm{SOC}=100\%}$ and $c_{s,\mathrm{k}}|_{\mathrm{SOC}=0\%}$), inevitably shift. Furthermore, the growth of the SEI layer directly increases the internal resistance. In our framework, the dynamically estimated Δn_{Li} is fed back into the model at every time step to continuously update both the boundary stoichiometries and the internal resistance (D. Yang, Wang, Pan, Chen, & Chen, 2017). This provides a deeply physical, closed-loop tracking of aging phenomena that is impossible to achieve with standard ECMs.
Consequently, the SOC is not a static calculation. It is defined as the volumetric average of the lithium concentration relative to the continuously updating stoichiometric bounds of the aged cell. For each electrode $\mathrm{k} \in \{\mathrm{n}, \mathrm{p}\}$, the volume-averaged concentration is computed as:

$$\bar{c}_{s,\mathrm{k}}(t) = \frac{\int_0^{R_\mathrm{k}} 4\pi r^2 c_{s,\mathrm{k}}(r,t)\, dr}{(4/3\pi R_\mathrm{k}^3)} \tag{17}$$

The specific SOC for each electrode is then mapped against its LLI-updated boundaries:

$$\mathrm{SOC}_\mathrm{k}(t) = \frac{\bar{c}_{s,\mathrm{k}}(t) - c_{s,\mathrm{k}}|_{\mathrm{SOC}=0\%}(\Delta n_{\mathrm{Li}})}{c_{s,\mathrm{k}}|_{\mathrm{SOC}=100\%}(\Delta n_{\mathrm{Li}}) - c_{s,\mathrm{k}}|_{\mathrm{SOC}=0\%}(\Delta n_{\mathrm{Li}})} \tag{18}$$

Finally, the global SOC of the cell is the average of the two electrodes:

$$\mathrm{SOC}(t) = \frac{\mathrm{SOC}_\mathrm{p}(t) + \mathrm{SOC}_\mathrm{n}(t)}{2} \tag{19}$$

This formulation ensures that the estimated SOC tightly reflects the true physical state of the battery, organically adjusting to capacity fade and structural aging without the need for standalone empirical degradation equations.

3. VALIDATION SETUP

3.1. High-Fidelity DFN Plant

In this work, the validation is carried out in a synthetic but high-fidelity environment. The plant is a DFN model of a graphite/NMC cell (Mohtat, Lee, Sulzer, Siegel, & Stefanopoulou, 2020), augmented with SEI growth, lithium plating, and loss of active material degradation mechanisms (X.-G. Yang, Leng, Zhang, Ge, & Wang, 2017). The full DFN plus degradation system was implemented and integrated in PyBaMM (Sulzer, Marquis, Timms, Robinson, & Chapman, 2021). The simulated plant outputs the terminal voltage, the electrode stoichiometries, and the LLI when a specific current profile is given. The LLI is used as the ground truth for the SOH estimation; the reference SOC is reconstructed from the electrode stoichiometries and inherently includes the effect of aging. The terminal voltage and the current available to the observers are corrupted by 1 mV and 1 mA Gaussian noise, respectively, in order to mimic typical onboard sensor accuracy.

3.2. ECM Baseline

As a benchmark for SOC-SOH co-estimation comparison, we consider a three-RC-branch Thevenin ECM embedded into a joint UKF, which represents the state of the art for industrial BMSs. We follow the formulation of (Plett, 2005): the model is a standard three-RC Thevenin network in which the OCV, the series resistance R_0, and the three pairs (R_i, C_i) are stored as 2D look-up tables in (SOC, T), identified offline from Hybrid Pulse Power Characterization (HPPC) pulses.
In the ECM-based observer, the SOH appears directly as an augmented state and enters the SOC dynamics as a slowly-varying capacity factor:

$$z_{k+1} = z_k + \frac{I_k\, \Delta t}{Q_{\mathrm{nom}}\, \mathrm{SOH}_k}, \tag{20}$$

$$\mathrm{SOH}_{k+1} = \mathrm{SOH}_k + w_{\mathrm{SOH},k}, \tag{21}$$

where z is the SOC, Q_{nom} is the beginning-of-life nominal capacity, Δt is the sampling interval, and w_{SOH} is a zero-mean Gaussian process noise whose variance encodes the expected rate of capacity fade per sampling step. The augmented state of the ECM-UKF therefore reads $\mathbf{x}_k^{\mathrm{ECM}} = [z,\, V_1,\, V_2,\, V_3,\, \mathrm{SOH}]_k^\top$, with V_1, V_2, V_3 the internal voltages of the three RC branches. The measurement equation is the standard Thevenin terminal-voltage law (OCV minus ohmic and RC drops), and the same voltage residual drives both the SOC and the SOH update.

3.3. Case Studies

Six case studies are considered, covering different ambient temperatures and load profiles:

- **CS1:** CC-CV charge / CC discharge (1 C) at 10°C.
- **CS2:** CC-CV charge / CC discharge (1 C) at 25°C.
- **CS3:** CC-CV charge / CC discharge (1 C) at 40°C.
- **DST1:** CC-CV charge / DST discharge at 10°C.
- **DST2:** CC-CV charge / DST discharge at 25°C.

- **DST3:** CC-CV charge / DST discharge at $40°$C.

The CS cases (CS1–CS3) evaluate the robustness of the joint estimator under constant load across the tested temperature range, while the DST cases (DST1–DST3) challenge both observers with highly dynamic, reversing load profiles representative of urban driving. In all scenarios, the cell is cycled continuously until the End-of-Life (EOL) criterion is met, defined as a residual capacity equal to 80% of the initial nominal capacity. To maintain tractable simulation times while thoroughly capturing the SOH dynamics, the kinetic constants of the degradation sub-models in the high-fidelity plant were proportionally accelerated. As a result, the CS cases reach EOL within approximately 120–150 Equivalent Full Cycles (EFC). Conversely, because the DST profiles entail a significantly longer duration and higher cumulative energy throughput per cycle, the EOL threshold is naturally reached in approximately 40 cycles.

Performance is quantified through two metrics:

- the Root Mean Square Error (RMSE) between the estimated and the reference SOC and SOH trajectories;
- the Coverage Width-based Criterion (CWC), which jointly penalizes the average width and the empirical coverage of the 2σ confidence interval produced by the UKF and provides a synthetic measure of the calibration of the uncertainty quantification.

Both metrics are computed separately for SOC and SOH and reported in Section 4.

4. RESULTS AND DISCUSSION

This section reports the joint SOC/SOH estimation performance of the proposed EM-based observer (EM-UKF) and of the benchmark ECM-based observer (ECM-UKF) on the six case studies CS1–CS3 and DST1–DST3. SOC results are summarized in Table 1, SOH results in Table 2. Representative time histories and aggregated performance plots are shown in Figs. 3-5.

4.1. CS1–CS3: CC-CV/CC Discharge at Varying Temperatures

The CS case studies (CS1, CS2, and CS3) share an identical load profile (a standard CC-CV charge followed by a 1C constant-current discharge) and differ only in ambient temperature, which is set to $10°$C, $25°$C, and $40°$C, respectively.

At the nominal temperature of $25°$C (CS2, Fig. 3), both observers track the reference SOC with reasonable accuracy. However, the EM-UKF demonstrates a clear advantage even under this relatively benign profile, achieving a cycle-averaged SOC RMSE of 0.28% compared to the ECM's 0.88%. The benefit of the physics-informed approach becomes significantly more apparent in the SOH trajectory. The LLI-augmented state of the EM-UKF converges smoothly to the reference capacity-fade curve with minimal bias (0.34% RMSE), whereas the ECM-UKF exhibits a noticeably higher SOH RMSE of 1.33%.

At off-nominal temperatures (CS1 and CS3), the performance gap between the two frameworks widens substantially. At first glance, it may seem counterintuitive that the ECM-UKF, which explicitly includes temperature-dependent parameters mapped via extensive HPPC testing, experiences such severe estimation degradation. However, this degradation exposes a fundamental limitation in the robustness of empirical observers. The UKF covariance matrices (process and measurement noise weights) for both models were tuned for optimal performance at the nominal $25°$C condition. As the cell ages at different temperatures, the rate of capacity fade (SOH drift) and the evolution of internal impedance change drastically. When the ECM encounters these unmodeled, temperature-accelerated aging dynamics, it lacks the structural physics to correctly interpret the resulting voltage residuals. Consequently, the ECM distributes the residual error erroneously between both the fast SOC and the slow SOH updates. This cross-contamination significantly increases the SOC RMSE and introduces severe bias into the SOH estimate. This is particularly evident at $10°$C (CS1), where the ECM-UKF SOH RMSE surges to 3.25% alongside a massive CWC score of 71.7, indicating heavily uncalibrated confidence intervals.

Conversely, the EM-UKF is fundamentally constrained by the mass-conservation laws embedded within its operator network training. These physical constraints naturally prevent the filter from making erratic, non-physical SOC corrections in response to temperature-induced voltage shifts. Instead, the residual voltage error is properly isolated and accommodated by the slow LLI channel, governed by the tightly constrained process noise on Δn_{Li}. As a result, the EM-UKF maintains a highly robust SOC RMSE of under 1.25% across the entire temperature range, while its SOH RMSE stays well below 1%. Across all constant discharge scenarios (CS1–CS3), the EM-UKF outperforms the ECM-UKF on every metric, proving that structurally embedded physics provides a level of operational robustness that empirical temperature-mapping cannot match.

Fig. 3 illustrates the SOH estimation comparison for the ECM's best-performing scenario (CS2 at $25°$C). As seen in the figure, the EM-based filter yields a significantly more confident and stable SOH trajectory compared to the ECM. Furthermore, the prominent SOH estimation error exhibited by the ECM between cycles 20 and 50 directly degrades its SOC tracking accuracy during that exact same period. This behavior confirms our earlier hypothesis regarding the inherent coupling of the two states within the observer: because the empirical ECM lacks a fundamental physical mechanism to separate slow capacity fade from transient voltage drops, errors in the SOH estimation inevitably cross-contaminate the fast SOC predictions.

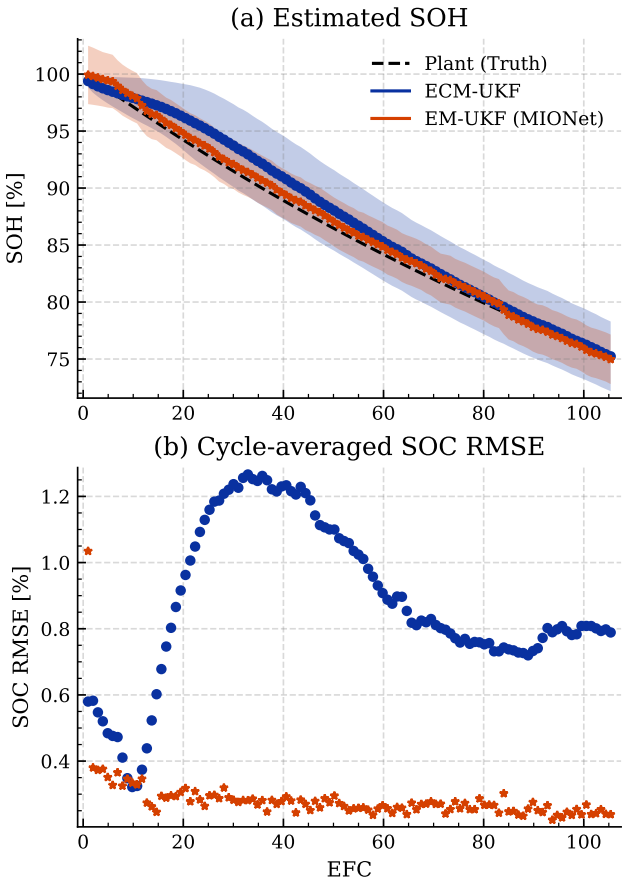

Figure 3. CS2 (25°C): (a) Estimated SOH and (b) per-cycle SOC RMSE.

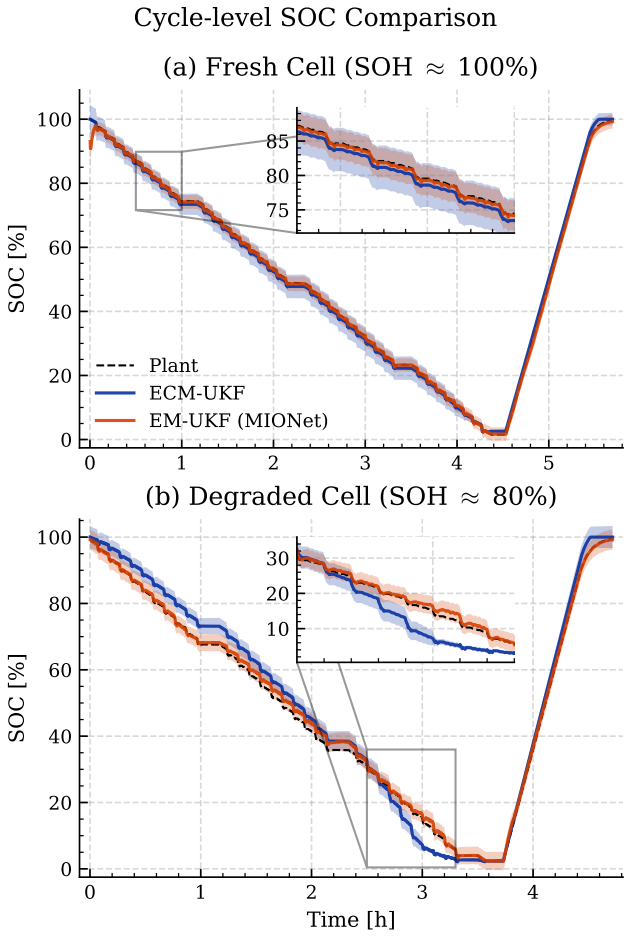

Figure 4. DST2 (25°C): SOC comparison for (a) fresh cell (SOH ≈ 100%) and (b) degraded cell (SOH ≈ 80%).

4.2. DST1–DST3: CC-CV/DST Discharge at Varying Temperatures

The DST cases (DST1–DST3) replace the constant-current discharge with the Dynamic Stress Test (DST) profile, which is characterized by rapid, reversing current pulses representative of urban traffic driving conditions. This highly dynamic profile presents a severe challenge for ECM-based observers, even for a fresh, unaged cell. Because the ECM is rigidly parameterized on specific HPPC excitations, it inherently lacks generalization capabilities outside of that narrow operating regime. Specifically, the static RC time constants identified from the HPPC pulses cannot adequately represent the broadband, frequency-dependent solid-phase diffusion dynamics excited by the DST profile. Consequently, the empirical state corrections produced by the UKF in the ECM framework end up being largely non-physical and highly erratic. In sharp contrast, the EM-UKF is built directly around the solution operator of Fick's law. The physics-informed surrogate naturally distinguishes between transient surface polarization (which drives immediate voltage spikes) and slow bulk concentration depletion, regardless of how chaotic the excitation spectrum becomes.

The numerical results presented in Tables 1 and 2 confirm this structural advantage quantitatively. Across the entire DST testing matrix, the EM-UKF drastically outperforms the ECM-UKF in both SOC and SOH estimation accuracy.

Figure 4 illustrates the SOC estimation comparison for the DST2 case study (nominal 25°C). Even in the earliest cycles, when the cell is fresh and unaged, the EM-UKF generates significantly narrower confidence bounds than the ECM-UKF. This indicates a much stronger statistical confidence in the state estimation, driven by the operator network's ability to precisely map the complex transient currents to valid concentration gradients. However, a completely different and more severe issue emerges during the cycles approaching the EOL of the battery. As the cell ages, unmodeled degradation phenomena—most notably the growth of internal resistance and the shifting of stoichiometric windows—begin to dominate the voltage response. Because the ECM relies on

static look-up tables that do not adapt to aging, this physical mismatch leads to massive errors in the SOC estimation. This severe late-life drift is the primary factor degrading the overall performance metrics (both RMSE and CWC) of the ECM in the DST case studies. The EM-UKF mitigates this drift by continuously feeding the estimated LLI back into the electrochemical model, physically updating the internal resistance and stoichiometric boundaries online, thereby maintaining tracking stability straight through to EOL.

4.3. Summary Tables and Confidence-Interval Analysis

Tables 1 and 2 summarize the SOC and SOH RMSE and CWC values for the two observers across the six case studies. The values reported in these tables represent the life-averaged metrics; for example, the SOC RMSE indicates the mean SOC estimation error calculated over the entire cycling life of the battery for that specific case study.

Table 1. SOC estimation performance: RMSE [%] and CWC for the six case studies.

	EM-UKF		**ECM-UKF**	
Case	RMSE [%]	CWC	RMSE [%]	CWC
CS1 (10°C)	1.25	7.1	1.40	14.2
CS2 (25°C)	0.28	5.1	0.88	10.8
CS3 (40°C)	1.05	5.5	1.92	7.1
DST1 (10°C)	1.75	15.6	2.42	74.3
DST2 (25°C)	1.04	5.0	2.39	71.1
DST3 (40°C)	0.79	5.0	1.67	13.6

Table 2. SOH estimation performance: RMSE [%] and CWC for the six case studies.

	EM-UKF		**ECM-UKF**	
Case	RMSE [%]	CWC	RMSE [%]	CWC
CS1 (10°C)	0.63	4.6	2.39	39.3
CS2 (25°C)	0.34	4.4	1.33	6.2
CS3 (40°C)	0.14	4.7	2.93	6.8
DST1 (10°C)	0.90	4.6	1.77	18.2
DST2 (25°C)	0.68	4.5	2.44	29.0
DST3 (40°C)	0.88	4.5	1.58	5.5

The CWC is constructed from two ingredients: the Prediction Interval Coverage Probability (PICP), which is the fraction of time during which the ground truth lies inside the estimated 2σ confidence band, and the Prediction Interval Normalized Average Width (PINAW), which measures how confident (i.e., narrow) that band is. As long as the PICP meets a target nominal coverage (95%, consistent with 2σ), the CWC reduces to the PINAW; if the PICP drops below the target, an exponentially growing penalty is added. The metric therefore rewards estimators that simultaneously stay close to the truth (high PICP) and keep their confidence intervals narrow (low PINAW), and severely punishes overconfident, biased estimators.

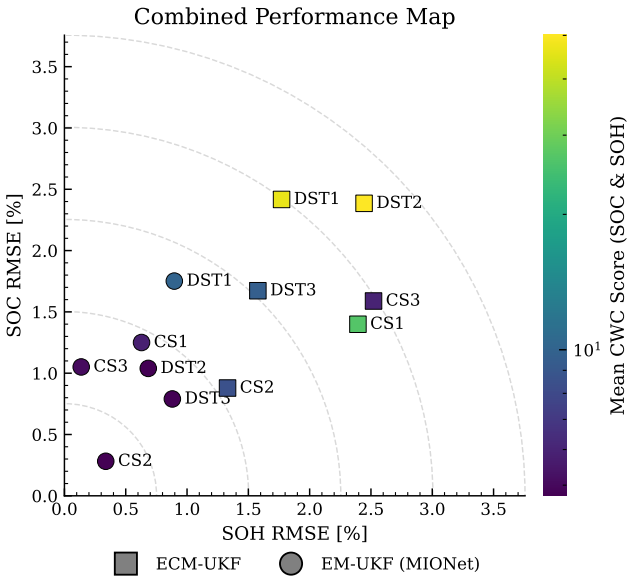

Figure 5. Combined SOC/SOH performance for the six case studies CS1–CS3 and DST1–DST3.

This is precisely what is observed in the tables. The EM-UKF systematically yields very low CWC values (typically between 4.4 and 7.1, with a worst case of 15.6 on DST1), which is the hallmark of an estimator that is at the same time accurate (the ground truth lies inside the confidence band) and confident (the band is narrow). This is exactly the desired behavior: when the confidence interval is narrow and yet the ground truth still lies within it, the BMS can rely on the estimate to make tight operating decisions. Conversely, the ECM-UKF reaches CWC values up to 71–74 in the most challenging cases (CS1 SOH, DST1–DST2 SOC). These figures are not dominated by wide confidence intervals, but by the exponential penalty triggered when the ground truth escapes the band: the ECM produces overly narrow confidence intervals around a drifting estimate, and the PICP collapses. Across all six case studies, the EM-UKF beats the ECM-UKF on both metrics for both states.

Finally, Fig. 5 summarizes the SOC and SOH estimation metrics from Tables 1 and 2 in a combined performance map. Each point represents the life-averaged metrics for a specific case study. The x-axis reports the SOH RMSE, while the y-axis shows the SOC RMSE. The color of each marker represents the CWC score of the estimation (for simplicity, computed as the mean between the SOC and SOH CWC scores), where darker shades correspond to lower CWC scores and thus higher statistical confidence. Furthermore, the concentric circumferences delineate equivalent combined performance levels, indicating the total distance from the ideal zero-error origin. Notably, the markers corresponding to the EM-UKF consistently lie further to the left and further down compared to the ECM-UKF. This spatial distribution visu-

ally demonstrates that the EM-UKF achieves, on average, simultaneously lower estimation errors for both SOC and SOH. Additionally, the EM-UKF points systematically exhibit darker colors, indicating that alongside higher accuracy, the EM-UKF yields more reliable and tighter confidence intervals than the traditional ECM approach.

5. CONCLUSIONS

In this work, we proposed a physics-informed framework for the joint, online estimation of SOC and SOH in Li-ion cells. Building upon a MIONet surrogate of the SPM, we formulated a joint UKF in which the spatial lithium concentration profiles of the electrodes and the LLI are augmented into a single state vector and co-estimated through the same terminal voltage measurement. SOH is recovered directly and algebraically from the estimated LLI. The framework was rigorously validated against a high-fidelity DFN plant—which included complex SEI growth, lithium plating, and loss of active material—across six representative lifecycle case studies spanning multiple temperatures and load profiles.

Across all scenarios, the EM-based observer consistently delivered lower SOC and SOH RMSE and substantially better-calibrated confidence intervals than the SOA ECM-based observer with an identical joint-UKF structure. While the ECM performed adequately under constant-current loads (CS1–CS3), its accuracy degraded significantly under highly dynamic, reversing load profiles (DST1–DST3), where its SOH RMSE more than doubled and its CWC score deteriorated by up to an order of magnitude compared to the EM-UKF. This performance gap is structural: the ECM compresses complex, multi-scale internal phenomena (fast surface polarization, charge-transfer kinetics, slow solid-phase diffusion) into static RC branches that fail to generalize to broadband dynamic excitations. Conversely, the MIONet surrogate natively separates these contributions by adhering to the underlying PDEs, proving highly superior in precisely the operating regimes that define real-world automotive use.

Furthermore, this superior performance is achieved while avoiding the massive empirical calibration burden inherent to ECMs. A full thermal map for an ECM requires hundreds of hours of dedicated laboratory HPPC testing, which must be repeated entirely if the cell chemistry or format changes. The physics-informed EM, relying on a unified set of fundamental electrochemical parameters, retains physical meaning and generalizes far better outside its immediate identification window.

The primary limitation of the proposed approach is the absence of an explicit SOH propagation model within the filter's prediction step. By design, the current formulation treats LLI purely as a random walk driven by measurement residuals. While this is sufficient for diagnosis, it leaves no room for forward-looking prognostics. Because our goal was to first isolate and demonstrate the feasibility of the surrogate EM for joint state tracking, we deliberately avoided introducing complex degradation sub-models.

The natural next step for this research is the integration of physics-based degradation models (e.g., explicit SEI layer growth and lithium plating kinetics) directly into the prediction step of the joint UKF. This will not only smooth the current diagnosis by providing prior knowledge on the rate of capacity fade, but it will also unlock the ability to propagate the model forward in time for true remaining useful life prognostics.

Ultimately, this work confirms that embedding physics into the estimator translates not only into superior benchmark metrics but also into a deeper, interpretable understanding of the system. Each component of the augmented state has a direct physical meaning constrained by conservation laws, making physics-informed estimators a powerful foundation for next-generation BMSs.

NOMENCLATURE

BMS	Battery Management System
CC-CV	Constant Current - Constant Voltage
CWC	Coverage Width-based Criterion
DFN	Doyle-Fuller-Newman Model
DST	Dynamic Stress Test
ECM	Equivalent Circuit Model
EFC	Equivalent Full Cycle
EM	Electrochemical Model
EOL	End of Life
EV	Electric Vehicle
GRF	Gaussian Random Field
HPPC	Hybrid Pulse Power Characterization
LLI	Loss of Lithium Inventory
MIONet	Multiple-Input Operator Network
MOR	Model Order Reduction
NMC	Nickel Manganese Cobalt
OCV	Open-Circuit Voltage
PDE	Partial Differential Equation
PICP	Prediction Interval Coverage Probability
PINAW	Prediction Interval Normalized Average Width
PINN	Physics-Informed Neural Network
RC	Resistance-Capacitance
RMSE	Root Mean Square Error
SEI	Solid Electrolyte Interphase
SOA	State of the Art
SOC	State of Charge
SOH	State of Health
SPM	Single Particle Model
UKF	Unscented Kalman Filter
UT	Unscented Transform

ACKNOWLEDGEMENTS

All source code, trained neural network weights, and post-processing scripts used in this study are publicly available at: https://github.com/HarejAl/PIMIONet-Joint-UKF-for-SOC-SOH-Estimation.git for reproducibility.

REFERENCES

Alanazi, F. (2023). Electric vehicles: Benefits, challenges, and potential solutions for widespread adaptation. *Applied Sciences*, *13*(10). Retrieved from https://www.mdpi.com/2076-3417/13/10/6016 doi: 10.3390/app13106016

Brancato, L., Harej, A. G., Giglio, M., & Cadini, F. (2026). Physics-informed operator learning for real-time battery state estimation. *Applied Energy*, *402*, 126987.

Chaturvedi, N. A., Klein, R., Christensen, J., Ahmed, J., & Kojic, A. (2010). Algorithms for advanced battery-management systems. *IEEE Control systems magazine*, *30*(3), 49–68.

Doyle, M., Fuller, T. F., & Newman, J. (1993). Modeling of galvanostatic charge and discharge of the lithium/polymer/insertion cell. *Journal of the Electrochemical society*, *140*(6), 1526.

Hu, X., Xu, L., Lin, X., & Pecht, M. (2020). Battery lifetime prognostics. *Joule*, *4*(2), 310–346.

Jin, P., Meng, S., & Lu, L. (2022). Mionet: Learning multiple-input operators via tensor product. *SIAM Journal on Scientific Computing*, *44*(6), A3490–A3514.

Krewer, U., Röder, F., Harinath, E., Braatz, R. D., Bedürftig, B., & Findeisen, R. (2018). Dynamic models of li-ion batteries for diagnosis and operation: a review and perspective. *Journal of the electrochemical society*, *165*(16), A3656.

Marquis, S. G., Sulzer, V., Timms, R., Please, C. P., & Chapman, S. J. (2019). An asymptotic derivation of a single particle model with electrolyte. *Journal of The Electrochemical Society*, *166*(15), A3693.

Mohtat, P., Lee, S., Sulzer, V., Siegel, J. B., & Stefanopoulou, A. G. (2020, jul). Differential expansion and voltage model for li-ion batteries at practical charging rates. *Journal of The Electrochemical Society*, *167*(11), 110561. Retrieved from https://dx.doi.org/10.1149/1945-7111/aba5d1 doi: 10.1149/1945-7111/aba5d1

Nuroldayeva, G., Serik, Y., Adair, D., Uzakbaiuly, B., & Bakenov, Z. (2023). State of health estimation methods for lithium-ion batteries. *International Journal of Energy Research*, *2023*(1), 4297545.

Plett, G. L. (2005). Dual and joint ekf for simultaneous soc and soh estimation. In *Proceedings of the 21st electric vehicle symposium (evs21), monaco* (pp. 1–12).

Sulzer, V., Marquis, S. G., Timms, R., Robinson, M., & Chapman, S. J. (2021). Python battery mathematical modelling (pybamm). *Journal of Open Research Software*, *9*(1).

Wan, E. A., & Van Der Merwe, R. (2000). The unscented kalman filter for nonlinear estimation. In *Proceedings of the ieee 2000 adaptive systems for signal processing, communications, and control symposium (cat. no. 00ex373)* (pp. 153–158).

Yang, D., Wang, Y., Pan, R., Chen, R., & Chen, Z. (2017). A neural network based state-of-health estimation of lithium-ion battery in electric vehicles. *Energy Procedia*, *105*, 2059–2064.

Yang, X.-G., Leng, Y., Zhang, G., Ge, S., & Wang, C.-Y. (2017). Modeling of lithium plating induced aging of lithium-ion batteries: Transition from linear to nonlinear aging. *Journal of Power Sources*, *360*, 28–40.

Zhang, R., Xia, B., Li, B., Cao, L., Lai, Y., Zheng, W., ... Wang, W. (2018). State of the art of lithium-ion battery soc estimation for electrical vehicles. *Energies*, *11*(7).